Supplemental material

Wang et al., https://doi.org/10.1083/jcb.201806191

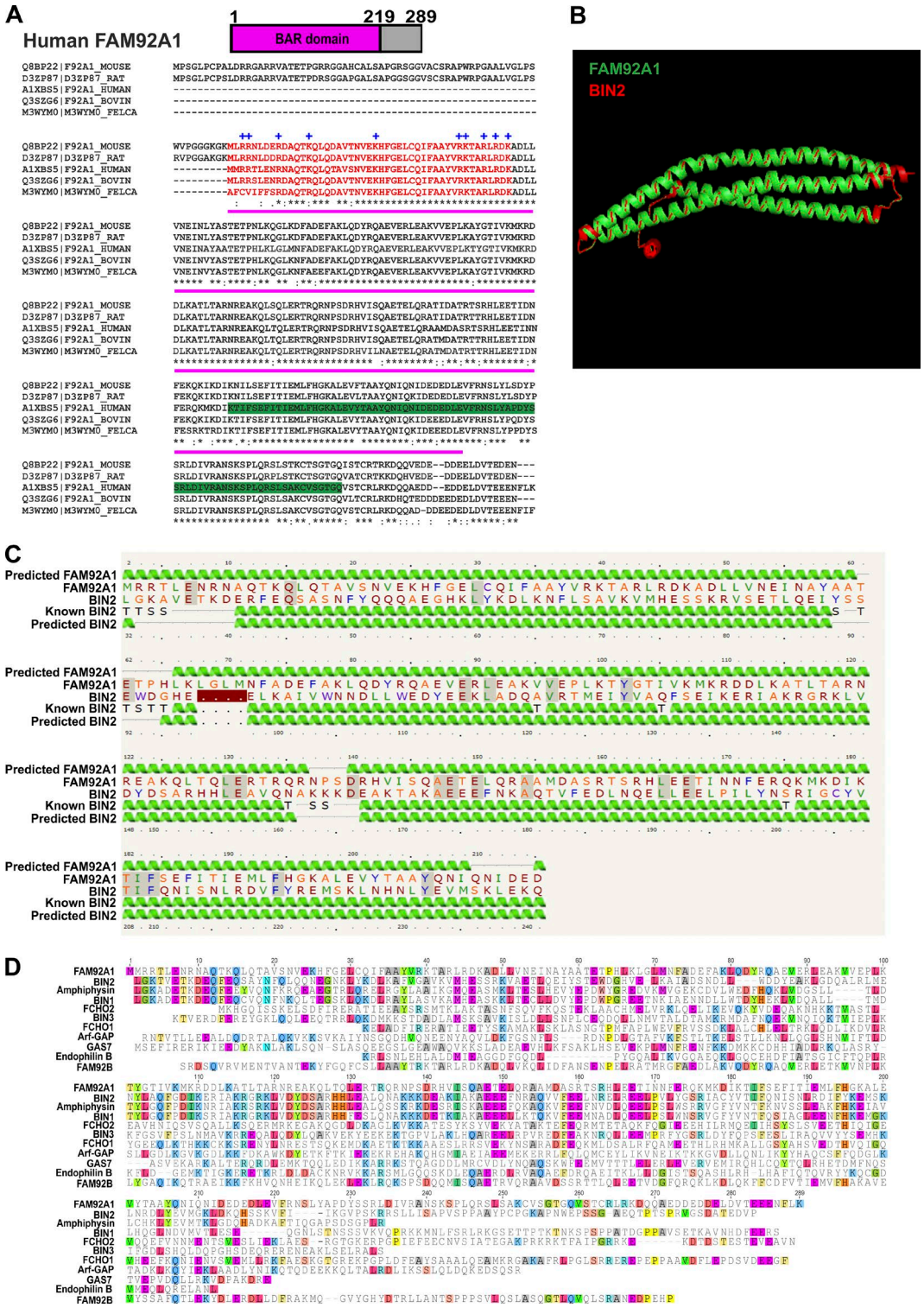

Figure S1. **FAM92A1 is a BAR domain protein. (A)** FAM92A1 is conserved in mammals revealed by multiple sequence alignment of FAM92A1 from human, mouse, rat, cow, and cat using the Clustal Omega server. The BAR domain is indicated with a magenta bar, and the N-terminal 47 aa is highlighted in red. The positively charged amino acids are indicated with plus signs. The specific FAM92A1 antibody–recognized sequence is indicated in green. **(B)** Structural similarity between the BAR domains of human bridging integrator 2 (BIN2; PDB: 4AVM) and FAM92A1 predicted by Phyre2. 73% of the FAM92A1 sequence (2–215 aa) was modeled with 99.95% confidence by the highest-scoring template BIN2. **(C)** Sequence alignment of FAM92A1 BAR domain with the BAR domain of BIN2. The BAR domain of FAM92A1 showed 10% primary sequence identity but high structural similarity with the BAR domain of BIN2. **(D)** Sequence alignment of FAM92A1 with 10 representative BAR domain protein sequences taken from Phyre2 PSI-BLAST results (407 total sequences). Some of these sequences have a 3D structure associated with them and have been used as templates in building a homology model for FAM92A1. The UniProt codes are FAM92A1 (A1XBS5), Amphiphysin (P49418), BIN1 (Q6P4W9), BIN2 (Q5ZKL7), BIN3 (Q9NQY0), FCHo1 (O14526), FCHo2 (Q502I9), Arf-GAP (Q9ULH1), GAS7 (O60861), endophilin B (Q8SYD9), and FAM92B (Q6ZTR7).

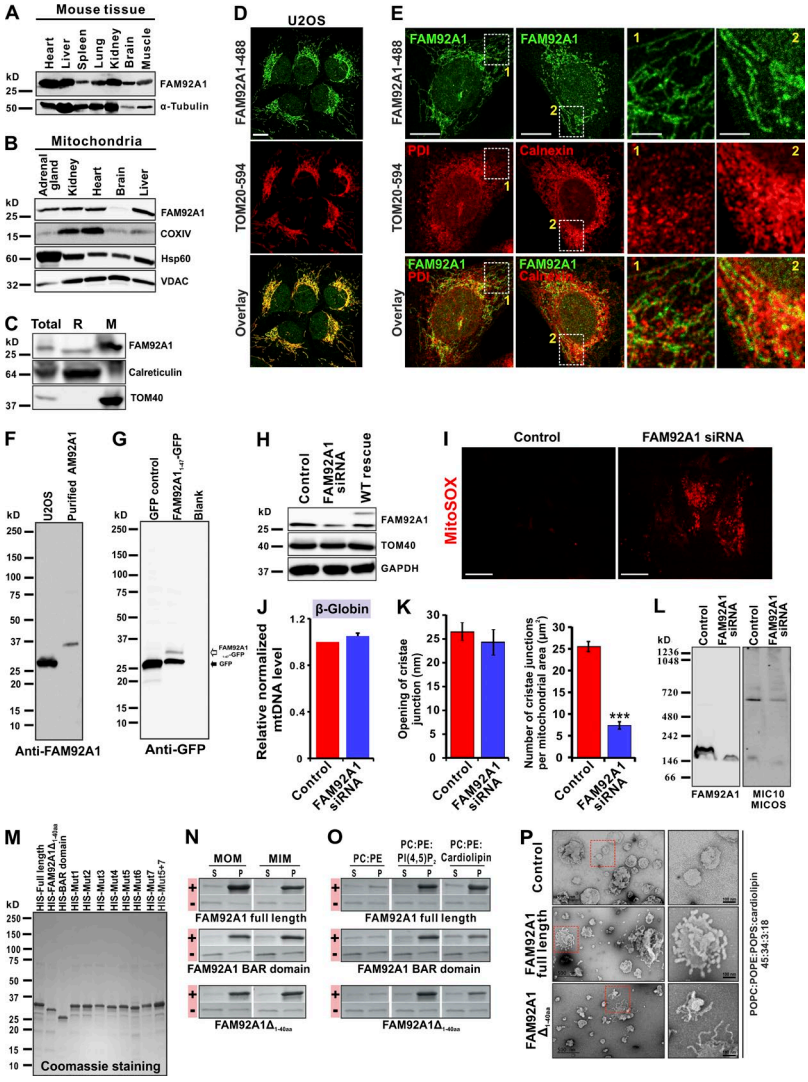

Figure S2. **FAM92A1 is a ubiquitously expressed mitochondrial protein that binds and remodels membranes. (A)** Western blot analysis of FAM92A1 expression in mouse tissues using a specific anti-FAM92A1 antibody. α-Tubulin was used as a loading control. **(B)** FAM92A1 was detected by Western blotting using a specific anti-FAM92A1 antibody in isolated mitochondria from rat adrenal gland, kidney, heart, brain, and liver, supporting that FAM92A1 is a ubiquitously expressed mitochondrial protein. COXIV, Hsp60, and voltage-dependent anion channel were used as mitochondrial internal controls. **(C)** FAM92A1 predominantly resided in the mitochondrial fraction (M). R represents the rest of cells except mitochondria. Cal reticulum and TOM40 were used as ER and mitochondrial protein controls, respectively. **(D)** Immunostaining of U2OS cells showed that the majority of FAM92A1 localized in mitochondria, with a minor localization in the cytoplasm and nucleus. The cells were immunostained with FAM92A1 and TOM20 antibodies. Bar, 10 µm. **(E)** Immunostaining of U2OS cells with FAM92A1 and ER protein antibodies. Bars: 10 µm (main images); 2.5 µm (insets). **(F)** Immunoblotting of endogenous FAM92A1 (~29 kD) and recombinant his-tagged FAM92A1 (~34 kD) using the anti-FAM92A1 antibody. Lanes 1 and 2 are the endogenous and recombinant FAM92A1, respectively. **(G)** Western blotting of FAM92A1$_{1–47}$-GFP after 24 h transfection. An anti-GFP antibody was used for immunoblotting. **(H)** Immunoblotting of cellular FAM92A1 level. The WT FAM92A1 was transiently expressed in cells after 20 h siRNA treatment. Cells were harvested for analysis after 48 h of FAM92A1 expression. The total siRNA treatment was 68 h. **(I)** Mitochondrial superoxide production in U2OS cells treated with FAM92A1 siRNA for 72 h, detected using a mitochondrial superoxide indicator MitoSOX for live-cell imaging. Bars, 20 µm. **(J)** Steady-state levels of mtDNA copy number in U2OS cells after treatment with control and FAM92A1 siRNA for 72 h detected by qPCR. The total mtDNA levels were normalized to β-globin levels. Error bars represent the mean ± SEM of three independent repetitions. **(K)** Quantification of cristae junction opening and numbers after FAM92A1 siRNA treatment for 72 h. ***, P ≤ 0.001, Student's *t* test. **(L)** Effects of FAM92A1 down-regulation on MICOS complex assembly detected by MIC10 antibody. **(M)** Coomassie staining of purified recombinant proteins. **(N)** Representative gel images of vesicle cosedimentation assay for the interaction of FAM92A1 with mitochondrial model membranes. The lipid compositions used for MOM and MIM were POPC:POPE:POPS:PI(4,5)P_2:liverPI:POPA:cardiolipin:RhodaminePE = 54:27:2:5:8:1:1:2 and POPC:POPE:POPS:PI(4,5)P_2:cardiolipin:RhodaminePE = 40:32:3:5:18:2, respectively. The protein controls shown were the loading controls and were deducted to get the actual binding percentage in quantification. P, pellet; S, supernatant. **(O)** Representative gel images of vesicle cosedimentation assays for the lipid-binding specificity assays of FAM92A1. The lipid compositions were POPC:POPE:RhodaminePE = 66:32:2, POPC:POPE:PI(4,5)P_2:RhodaminePE = 48:32:18:2, and POPC:POPE:cardiolipin:RhodaminePE = 48:32:18:2. The final protein and lipid concentrations used in C and D were 2 and 500 µM, respectively. The corresponding protein controls shown are the same as in N (MIM), which were the loading controls and deducted to get the actual binding percentage in quantification. **(P)** Membrane tubulation of MIM lipid composition without PI(4,5)P2 after mixing with full-length FAM92A1 and FAM92A1Δ1-40aa, analyzed by transmission electron microscopy. The lipid composition was POPC:POPE:POPS:cardiolipin = 45:34:3:18. The final concentrations of FAM92A1 and lipid were 2 and 500 µM, respectively.

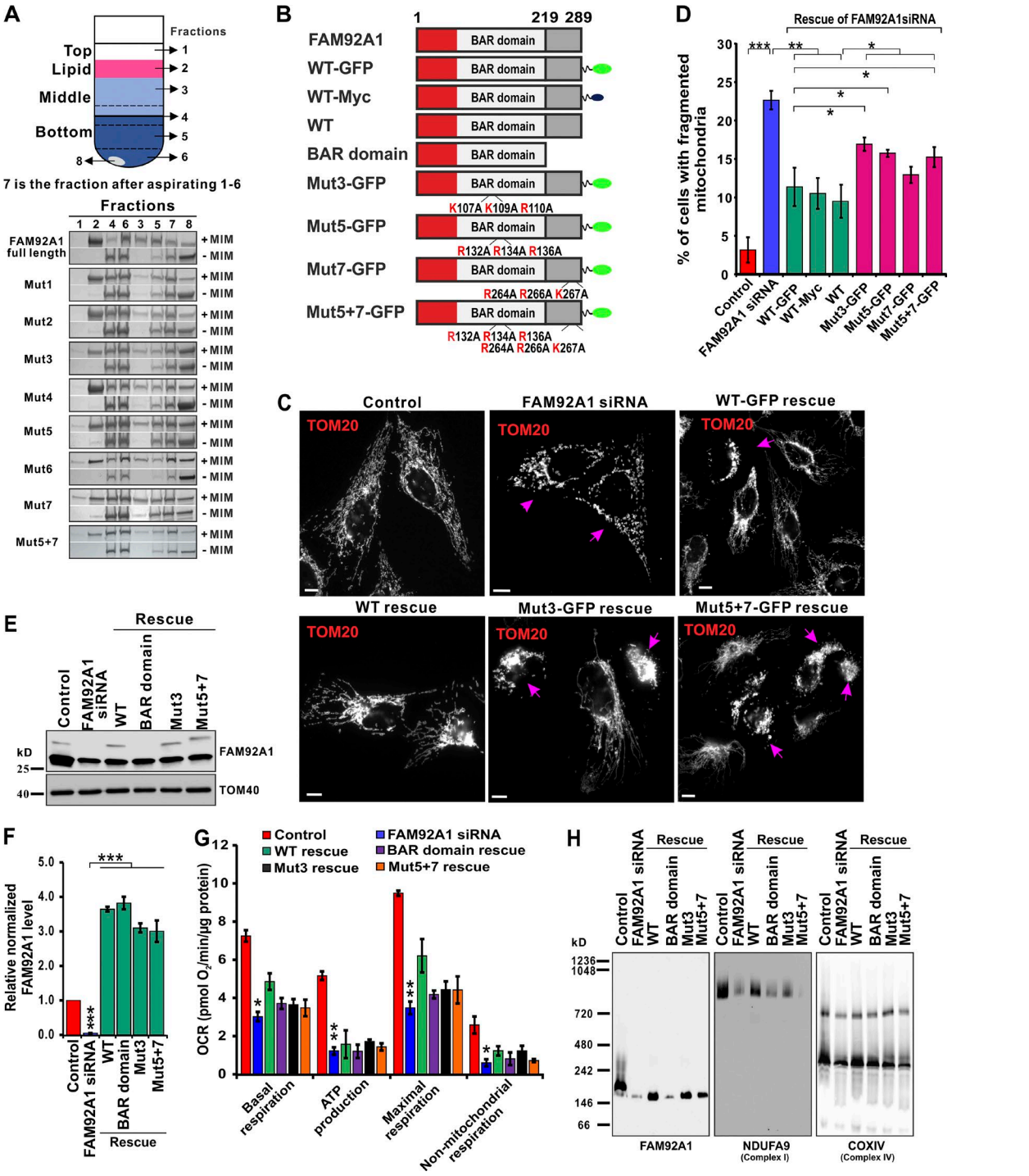

Figure S3. **Rescue of mitochondrial morphology by WT FAM92A1 and mutants with defects in membrane binding and remodeling. (A)** Schematic diagram of vesicle coflotation assay (top) and representative gel images (bottom). After ultracentrifugation, 100-µl fractions were collected from top to bottom (fractions 1–8), and the samples were run on SDS-PAGE. The membrane binding was calculated using the protein intensity in the liposome fraction (fraction 2) divided by the intensity sum of all the fractions. The protein control was deducted to get the actual membrane binding. The final protein and lipid concentrations used were 2.5 and 333 µM, respectively. The lipid composition for MIM was POPC:POPE:POPS:PI(4,5)P_2:cardiolipin:RhodaminePE = 40:32:3:5:18:2. **(B)** Schematic diagram of FAM92A1 and mutants with/without a tag. **(C)** Representative fluorescence images of U2OS cells after expressing the rescue constructs for 24 h in FAM92A1-depleted cells. Mitochondria were labeled with anti-TOM20 antibody and visualized by secondary antibody conjugated with Alexa Fluor 594. Bars, 10 µm. The arrows indicate the abnormal mitochondria. **(D)** Quantification of mitochondrial morphology after reexpressing 24 h WT FAM92A1 or mutants in FAM92A1-knockdown cells. At least 200 cells were used for analysis. **(E)** Immunoblotting analysis of FAM92A1 protein levels. **(F)** RT-qPCR detected the transcription level of FAM92A1. **(G)** Statistical analysis of OCR in FAM92A1-knockdown cells and rescue of OCR changes by WT FAM92A1 and mutants. **(H)** Effects of FAM92A1 down-regulation on the complex assembly of complexes I and IV and rescue of complex assembly changes by WT FAM92A1 and mutants. In C–H, WT FAM92A1 and mutants were transiently expressed in FAM92A1-depleted cells after treatment with FAM92A1 siRNA for 20 h. Cells were harvested after 24 h expression of rescue constructs. *, P ≤ 0.05; **, P ≤ 0.01; ***, P ≤ 0.001, Student's *t* test.

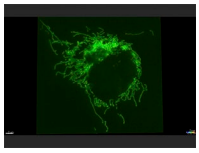

Video 1. **Mitochondrial dynamics in U2OS cells expressing mito-YFP after 72 h control siRNA treatment.** The video was acquired with a Marianas imaging system at 5 s/frame.

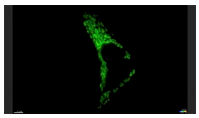

Video 2. **Mitochondrial dynamics in U2OS cells expressing mito-YFP after 72 h FAM92A1 siRNA treatment.** The video was acquired with a Marianas imaging system at 5 s/frame.

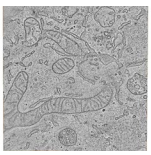

Video 3. **Mitochondria display normal cristae architecture in control U2OS cells.** Mitochondria were viewed from the top. The models are shown in perspective mode, thereby the scale bars apply to the center of the images.

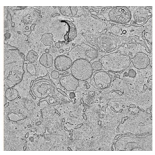

Video 4. **Silencing of FAM92A1 caused severe changes in mitochondrial ultrastructure.** Cristae became disorganized, and the cristae width and length were significantly changed. Mitochondria were viewed from the top. The models are shown in perspective mode, thereby the scale bars apply to the center of the images.

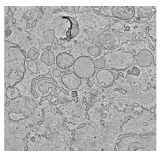

Video 5. **Silencing of FAM92A1 caused severe changes in mitochondrial ultrastructure.** Mitochondria in FAM92A1 cells had reduced cristae contents along with very short and wide cristae. Mitochondria were viewed from the top. The models are shown in perspective mode, thereby the scale bars apply to the center of the images.

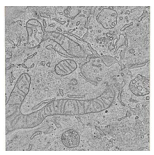

Video 6. **Mitochondria display normal crista junction in control U2OS cells.** Mitochondria were viewed from the side. The models are shown in perspective mode, thereby the scale bars apply to the center of the images.

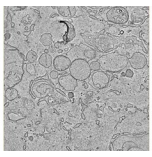

Video 7. **Silencing of FAM92A1 caused changes in mitochondrial crista junctions.** The crista junctions became disorganized. Mitochondria were viewed from the side. The models are shown in perspective mode, thereby the scale bars apply to the center of the images.